Chapter 11

# Fluorinated Graphene Dielectric and Functional Layers for Electronic Applications

Irina V. Antonova and Nadezhda A. Nebogatikova

Additional information is available at the end of the chapter

http://dx.doi.org/10.5772/67451

**Abstract**

Future electronics technology is expected to develop from rigid to flexible devices. This process requires breakthroughs in material properties, especially flexibility, in combination with desirable electrical insulating, semiconducting, or metallic properties. Graphene, being one of the recently developed two-dimensional (2D) materials, presents great promise as an active layer in a wide spectrum of electronics devices and, first of all, in field-effect transistors (FET). The development of optimized dielectrics for the graphene active layer is critical for graphene applications. The carrier transport in graphene films takes place at interfaces with dielectric or semiconductor substrates; therefore, the quality of such interface and the interaction of graphene films with nearby dielectric layers (charge carrier scattering) determine the device performance. Generally, the development of dielectric materials aiming at high performance device operation, proper mechanical properties, and low-temperature fabrication is not progressing well since the graphene thin film is very sensitive to surface conditions of dielectric layers. Solving the problem with dielectric layers in the case of nonorganic printed and flexible electronics is especially acute. As it is demonstrated in the present chapter, dielectric layers fabricated from fluorinated graphene suspension or in its combination with graphene oxide are the most promising for graphene-based flexible, printed, and transparent electronics.

**Keywords:** flexible electronics, fluorinated graphene, suspension, dielectric films, leakage current, charges, resistive switching, quantum dots, negative differential resistance

## 1. Introduction

Future technologies evolve toward flexible electronics (bendable, rollable, stretchable, or transparent) developed for a wide spectrum of bio- and medical applications, sensors and gadget displays, textile or clothing electronics, and so on [1–4]. Printing processes have attracted great attention, due to their compatibility with flexible substrates and materials, excellent prospects for

applications, technical feasibility for scaling to large-area manufacturing and low cost. The two-dimensional (2D) printing technologies are at present used for creating intelligent components and smart systems of printed electronics, such as memories, displays, electronics, batteries, micromechanical systems, sensors, thin-film transistors, and other devices of modern electronics [1–4]. Flexible device technology does not support high temperatures, required for such materials as $SiO_2$ or high-k $Al_2O_3$, $HfO_2$, and $ZrO_2$ [5]. So, alternative 2D dielectric materials are highly demanded. Recent developments in technologies of liquid-phase graphene exfoliation lead to a significant progress in methods for creating 2D materials, including graphene, graphene oxide (GO), and other related materials ($MoS_2$, $WSe_2$, and so on) [6–10].

Graphene presents great promise as an active layer in a wide spectrum of devices of flexible electronics and, first of all, in field-effect transistors. Recent reports demonstrate successful realization of graphene FETs on flexible or even on stretchable substrates [8–13]. To make such applications possible, the development of optimized dielectrics for the active graphene layer is critical (gate and interlayer dielectrics, or/and supported layer for graphene). Nowadays, traditional high-k materials, such as $Al_2O_3$, $HfO_2$, and $ZrO_2$, are widely used for FETs. Nevertheless, the development of dielectric materials allows achieving high performance of the devices with excellent mechanical properties and low fabrication temperature that is in great demand.

Recently, graphene oxide (GO), one of the most well known graphene derivatives, has been exploited as a gate dielectric for graphene-based FETs [7, 8, 12, 13]. With its good mechanical and optical properties, this material offers a unique advantage for high performance flexible and transparent electronic devices since it can be formed on a graphene channel by solution-based or direct oxidation at room temperatures. Generally, GO has combined an excellent flexibility, a relatively large leakage current, and a strong limitation on enhanced temperature (even under the current flow). This limitation on enhanced temperature is connected with reducing GO: for instance, annealing at 100 °C typically leads to a decrease in GO layer resistivity by 4–5 orders of magnitude [5].

The most stable graphene derivative with dielectric properties is fluorinated graphene (FG), which is a low-k material with k = 1.2 and band gap of 3–8 eV [14–16]. Graphene can be fluorinated by a low-damaged $CF_4$ plasma treatment [16] or by exposing the graphene to $XeF_2$ gas to convert it to insulating fluorographene ($C_4F$) [17]. A new simple approach for graphene fluorination (treatment in aqueous solution of hydrofluoric acid) was recently suggested in Refs. [18, 19]. In the case of graphene suspension, such treatment leads not only to fluorination of flakes but also to additional flake fragmentation and exfoliation [19, 20]. As a result, a considerable decrease in thickness and lateral sizes of graphene flakes is accompanied by simultaneous transition of the flakes from conducting to insulating state. Smooth and uniform insulating films with low roughness can be created from the suspension on different substrates. The films from the fluorinated suspension are cheap, practically feasible, and easy to produce. The electrical and structural properties of the films from such fluorinated suspension with variable fluorination degree are discussed in the present chapter. Excellent characteristics of the dielectric film created from high fluorinated FG may be compared only with well developed $SiO_2$ layers. In addition to excellent dielectric properties, reversible resistive switching effect and negative differential resistance (NDR) were detected in the films, created from the suspension with relatively low fluorination degree. Possible applications of these films are also considered.

http://dx.doi.org/10.5772/67451

## 2. Fluorination of graphene suspensions

The starting material was a graphene suspension that can be obtained using any of available approaches. It may be suspensions created by mechanical crushing of natural graphite, dimethylformamide (DMF) intercalation, ultrasonic treatment intended for splitting the intercalated particles, and centrifugation aiming at removal of nonsplit graphite particles [20]. At the stage of intercalation, other organic solvents may be used, for instance, N-methyl-2-7 pyrrolidone (NMP) [21, 22]. Suspensions may be also created by electrochemical exfoliation [23, 24], liquid-phase exfoliation in water or water-based solution [25], or shear mixer [26, 27]. During suspension preparation, the natural graphite typically turned into flakes with characteristic size from 1 to several micrometers and thickness from 0.4 (monolayer) up to tens of nanometres. Parameters of flakes strongly depend on the technology used. After obtaining the suspension, it was subjected to a fluorination procedure [20, 28]. To this end, equal volumes of the suspension and a 5–10 % solution of hydrofluoric acid (HF) in water were mixed together. Fluorination time strongly increased with an increase in size and thickness of pristine graphene flakes and could be accelerated by enhancing temperature [20]. Below, we demonstrate the fluorination process in the time scale when pristine graphene flakes have lateral sizes of 1–2 mm and thickness of 3–20 nm, without temperature acceleration. So, we are considering the admittedly inferior option which took sufficiently long time to clarify fluorination stages and all accompanying processes.

Let us consider here the reason for graphene fluorination during treatment in the aqueous solution of hydrofluoric acid (HF treatment). It is very important to note that practical difficulties associated with F reactions in two-dimensional (2D) carbon nanostructures are avoided if working with curved carbon nanosheets. An example of F reactions with corannulene molecules having a curved surface representing 1/3 of the structure of $C_{60}$ fullerene was realized by dos Santos [29]. Corannulene is a polycyclic aromatic hydrocarbon with chemical formula $C_{20}H_{10}$. Density functional theory (DFT) calculations of the HOMO−LUMO were used to demonstrate that gap variation for fluorinated corannulene, used as a prototype of C-based nanostructures, yields in values of band gap of 0.13–3.46 eV due to fluorination. Our experiments on the fluorination of CVD grown or mechanically exfoliated graphene in the aqueous solution of hydrofluoric acid also show corrugation of these materials during fluorination. In other words, the corrugation of domain boundaries is an initial driving force for subsequent F reaction with carbon atoms in 2D plain and subsequent corrugation [19, 30–32]. This type of reactions stimulated by deformations is also realized for the graphene suspension, and only thin (few layer) flakes are suitable for fluorination during HF treatment.

Liu et al. [33] have employed the first-principles method within the density functional theory to study the structural, electronic, and magnetic properties of the fluorinated graphene with different coverage of fluorine. The authors have found a strong variation of the graphene properties already at the early stage of fluorination (lower than $CF_{0.25}$). Duan [34] has demonstrated that when fluorine bonds to a carbon atom, the latter one is pulled slightly above the graphene plane, creating what is referred to as a CF defect. These CF defects cause the graphene surface buckling. This corrugation was experimentally observed under fluorination in the aqueous solution of the hydrofluoric acid [33]. Duan further showed that the addition of

fluorine to graphene in some cases leads to the formation of an energy band gap near the Fermi level of 0.37–0.24 eV [34]. Generally, it was demonstrated that the adsorption of fluorine on graphene surfaces is a promising approach to modify the properties of graphene, which may lead to more flexible electrooptical applications of graphene in the future.

To investigate the properties of FG suspension, some portions of the suspension were periodically used for the study and preparation of films. The substrates for films were silicon (Si) wafers. In depositing the films, the native oxide was removed from the surface of silicon by the hydrofluoric acid available in the solution. The deposited films were dried and rinsed with deionized water for removing the residual hydrofluoric acid and the organic component of the suspension, and then subjected to a second drying treatment for water removal. In other cases (especially for 2D printing), the solution in suspension was substituted for water. Due to hydrophilicity of FG flakes, the water-based suspension was stable.

## 3. The evolution of graphene suspension structure during fluorination

Fluorination of the DMF-based graphene suspension with a solution of hydrofluoric acid in water is considered in the present part. It has been found that, as a result of the interaction, the suspension particles undergo an additional splitting and size reduction by one-two orders of magnitude. **Figure 1(a)–(d)** shows the surface image of films created of Si substrate from the suspension after different times of fluorinated treatment. A schematic pattern for the action of the HF-containing solution on suspension particles resulting in additional exfoliation of graphene sheets, and formation of thinner and finer fluorinated graphene flakes has been proposed (**Figure 1(e)**). The driving force of these structural changes is found to be mechanical stresses, due to a difference in lattice constants and wettability of fluorographene [20, 28]. The similar fragmentation and exfoliation of graphene flakes are found for different kinds of graphene suspensions during the fluorination process.

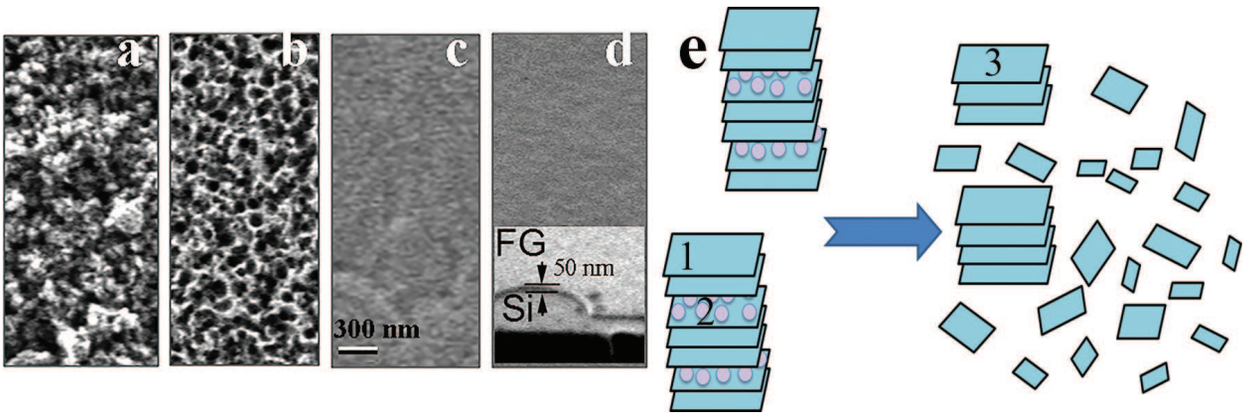


**Figure 1.** Scanning electron microscopy (SEM) images of the surface for films with different fluorination degree: (a)—pristine (nonfluorinated) film; (b), (c), and (d)—films fluorinated respectively during 2, 10, and 40 days. The inset in (d) shows an image of an edge of the film taken at the angle of 45° to the surface; the film thickness indicated in the figure was evaluated with allowance for measurement geometry. (e) A sketch illustrating initial flakes splitting and their fractionation in finer flakes that occurred during fluorination process (1—initial particle, 2—split of partially fluorinated flakes, 3—intercalated DMF layer). Reprinted with permission from Ref. [20].

http://dx.doi.org/10.5772/67451

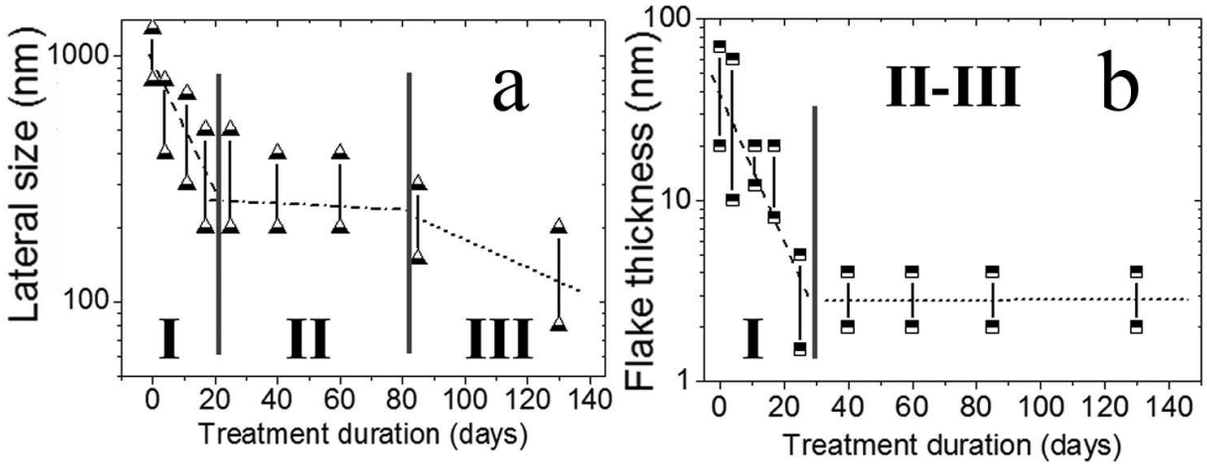


**Figure 2.** Dependence of the lateral size and thickness of multilayered graphene flakes in suspension with optimum composition of 0.16 mg/ml on fluorination time. Reprinted with permission from Ref. [28].

Dependences of FG flake size on time of HF treatment are given in **Figure 2**. It is seen that the process of flakes fragmentation may be divided into several stages—up to 20 days, from 20 to 80 days, and over 80 days. These intervals correlate with changes in electrical properties of the films obtained from suspensions. About 20-day treatment was required for the film transition from conducting to insulating state. During fluorination for 20 to 80 days, the insulating properties of the films improved, and the current through the films and the charge density in the films decreased. As it will be demonstrated below, the most optimal property for the majority of applications is the fluorination within 60–80 days. The observed stages well agree with the behavior of leakage current through the FG film, which are also given below (**Figure 4(a)**).

Evidences proving the fluorination of suspension particles during the suspension treatment in a solution of HF in water were obtained by means of analysis techniques such as X-ray photoelectron spectroscopy (XPS), Fourier transform infrared (FTIR) spectroscopy, and Raman scattering spectroscopy (RSS) (**Figure 3(a)** and **(b)**) [17]. Strong IR bands with maxima 1107, 1166, and 1230 $cm^{-1}$ are clearly seen in the FTIR spectra. The observed modes supposedly correspond to the fluorine atoms, connected with $sp^3$-hybridized carbon atoms. The studies of FTIR spectra with an increasing fluorination time have revealed that an adsorption band at 1112 $cm^{-1}$ gradually changes into 1211 $cm^{-1}$. The modes observed for the studied films are supposed to correspond to C-F bond and change depending on fluorination time. The gradual emergence of fluorinated graphene properties was traced in measured Raman spectra (**Figure 3 (b)**) for the films, which was obtained from suspensions with different fluorination times. It is seen that an increased duration of the treatment results in a decreased intensity of peaks in Raman spectra. This effect is typical for fluorination of graphene and connected with band gap opening. The images of pristine graphene suspension and FG suspension also clarify the fluorination process. XPS spectra show a signal from fluorine F1s and carbon C1s, detected in the energy region of 687.7 and 284–286 eV, respectively (**Figure 3(d)**). The energy position and shape of the peaks are indicative of partial fluorination of suspension particles. Decomposition of C1s demonstrates peaks C-F with position at 288.3 eV and a peak C-CF at 286.5 eV. These XPS spectra correspond to fluorination degree ~ $C_4F$ and are typical for the case when suspension becomes transparent and transfers to a nonconductive state (see details in Section 6). In a

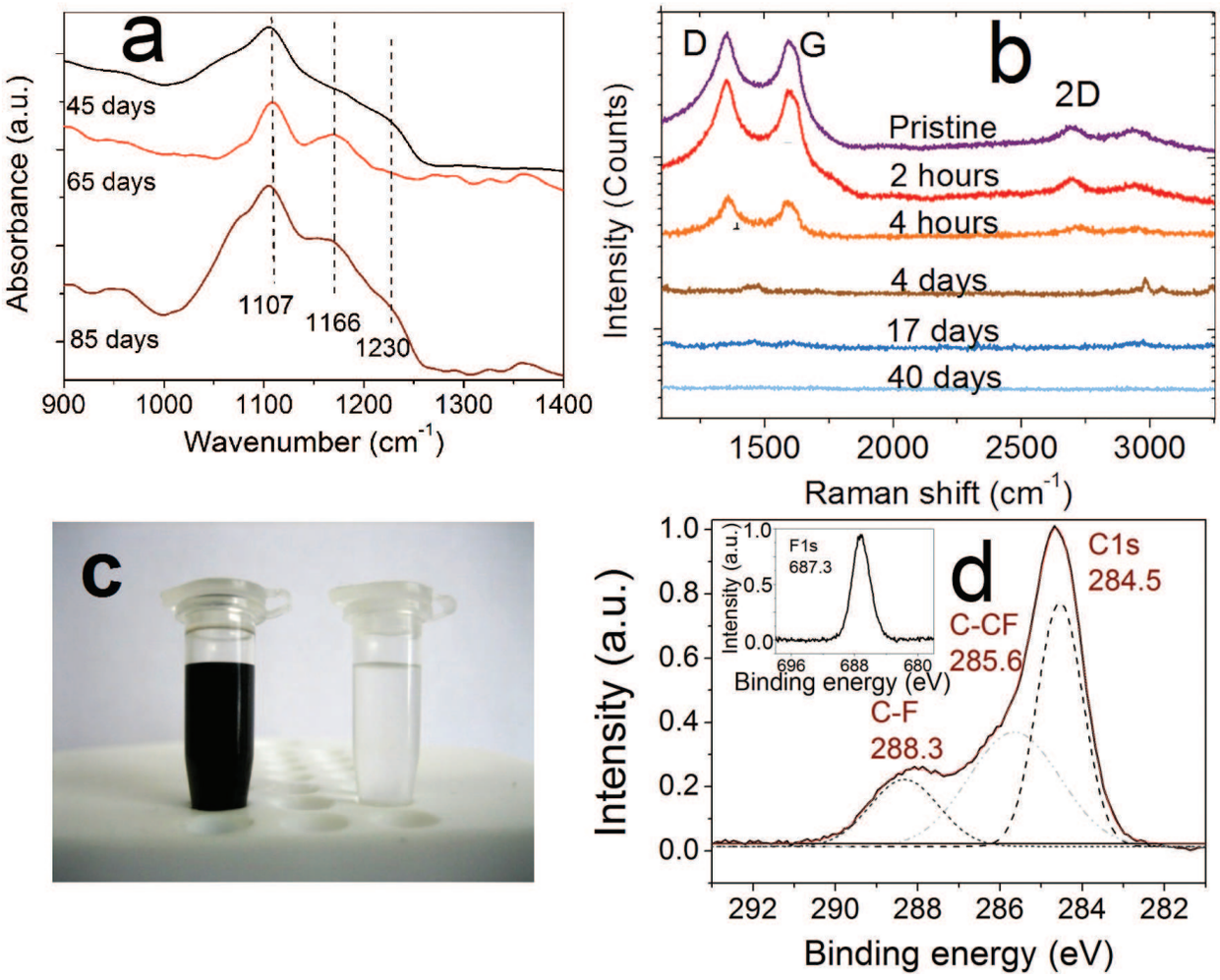


**Figure 3.** (a, b) Evolution of IR and Raman spectra of pristine fluorinated films with time of HF treatment. (c) Images of pristine graphene suspension and FG suspension after 50 days of HF treatment. (d) XPS study of the fluorinated graphene film: the spectrum near the peak of C1s with decomposition into component lines, an insert shows a part of the spectrum with F1s peak. Fluorination time was 50 days. Reprinted with permission from Ref. [20].

longer HF treatment, it is possible to obtain higher fluorination degrees limited to the value ~ $C_2F$. Due to this fact, we have a partially fluorinated suspension in all cases, and namely this FG suspension demonstrates many properties that are attractive for applications.

## 4. Insulating properties of hardly fluorinated graphene suspension

As it has been shown earlier, a considerable decrease in thickness and lateral sizes of graphene flakes (up to 1–5 monolayers in thickness and 20–30 nm in diameter) during fluorination is found to accompany the transition of the grapheme flakes from conducting to insulating state. The change in leakage current through the FG films as a function of the fluorinated time is given in **Figure 4(a)**. One can compare these currents with leakage current of 17 mA/cm$^2$ for 100 nm thick GO films [12] and ~20 A/cm$^2$ for 4 nm GO films [8]. So, the electrical and structural properties of the films suggest their use as insulating elements in thin-film nano- and microelectronics devices/structures. We have performed an analysis of the capacitance-

http://dx.doi.org/10.5772/67451

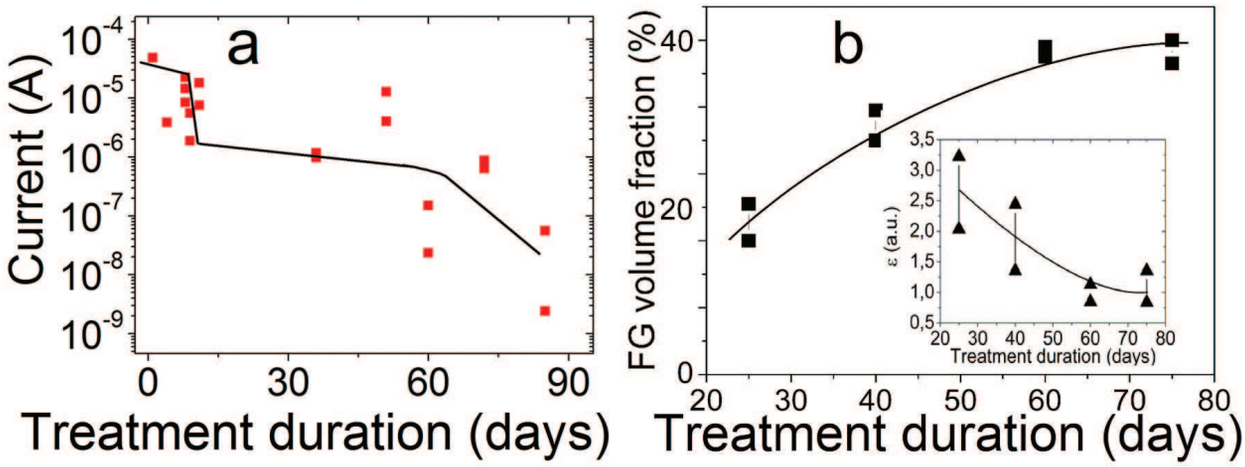


**Figure 4.** (a) The electric current density across the vertical Me/FG film/Si structures biased with voltage U = ± 0.1 V versus the duration of the suspension fluorination procedure. (b) Film fluorination degree versus the duration of fluorination treatment in the solution of HF in water. The inset in (b) shows the value of dielectric constant ε versus the fluorination treatment duration. (b) is reprinted with permission from Ref. [20].

voltage characteristics of metal (Ag, Au)/insulator (FG)/semiconductor (Si) (MIS) structures on different substrates. Dependence of relative dielectric constant ε on fluorinated time is shown in **Figure 4(b)**. The dielectric constant of the films is determined to range from 1.1 to 3.2, depending on the fluorination degree of the material. It is important to mention that value of ε = 1.2 known for fluorographene [16, 20], appears in our films for relatively low fluorinated degree (between $C_4F$ and $C_2F$).

The density of the fixed charge in the film $Q_f$ extracted from the flat band voltage of the capacitance-voltage characteristics and the density of interface states at the interface with silicon $D_{it}$ are given in **Table 1**. Recall that the fluorinated graphene film was applied onto a silicon surface free of native oxide. The densities $Q_f$ and $D_{it}$ proved to range from $6 \times 10^{11}$ $cm^{-2}$ to $(0.3–0.5) \times 10^{11}$ $cm^{-2}$. With increasing duration of fluorination treatment, the densities $Q_f$ and $D_{it}$ were found to decrease in value. The quality of obtained dielectric films was improved by increasing the treatment duration. On the whole, the obtained values proved to be much lower than the values of $Q_f$ and $D_{it}$, typical of many traditional dielectric coatings used in nano- and microelectronics such as $Al_2O_3$, $HfO_2$, and $ZrO_2$ [5]. The typical values of built-in or interface charge density in the widely used $Al_2O_3$ films range within $10^{12}$–$10^{13}$ $cm^{-2}$ [35]; in $HfO_2$, they vary within $10^{11}$–$10^{12}$ $cm^{-2}$ [36, 37], and in the Si/$SiO_2$graphene/$ZrO_2$ structures, they range within $(1–15) \times 10^{11}$ $cm^{-2}$ $eV^{-1}$ [38].

| Substrate | Time of HF treatment | 20 days | 40 days | 60 days | 80 days | 150 days |
|---|---|---|---|---|---|---|
| Si | $Q_f$, $cm^{-2}$ | $(5–6) \times 10^{11}$ | $1 \times 10^{11}$ | $5 \times 10^{10}$ | $(2–6) \times 10^{10}$ | $(5–7) \times 10^{10}$ |
| Si | $D_{it}$, $cm^{-2}$ | $(3–5) \times 10^{11}$ | $5 \times 10^{10}$ | $(1–3) \times 10^{10}$ | $2 \times 10^{10}$ | $(3–5) \times 10^{10}$ |

**Table 1.** Specific values of fixed charge density $Q_f$, calculated on the flat band voltage, determined from the capacitance-voltage characteristics, and the state density $D_{it}$ at the interface with silicon, obtained from the difference between the middle-gap and flat band voltages.

## 5. Relation between structural and electronic properties of FG films

**Figure 5** shows SEM and AFM images of partially fluorinated films, created from the graphene suspension, treated in an aqueous solution of HF for 7 days (~$CF_{0.10}$) and 20 days ($CF_{0.23}$) [31]. In both cases, the continuous films consisting of separate flakes may be observed in **Figure 5**. The bright corrugated areas of the film correspond to fluorinated regions, and the dark round regions correspond to nonfluorinated or weakly fluorinated graphene islands. The estimated flake sizes in suspension are 100–300 nm with a thickness of 0.5–5 nm for less fluorinated films (see **Figure 2(a)** and **(b)**), and 20–100 nm with a thickness of 0.5–2 nm for more fluorinated ones. The film thickness varies from 20 to 150 nm depending on the drop volume. **Figure 5(a)** and **(b)** presents the AFM image and the current map, measured with the probe for the same part of the weakly fluorinated FG film. Conductivity was found for graphene islands (dark areas), and bright areas (fluorinated part) were characterized by insulating properties. A comparison of AFM images clearly demonstrates that an increase in the HF treatment time leads to a decrease in the size of graphene islands and an increase in the size of the fluorinated areas between the graphene islands. So, generally, the films contain graphene islands and their properties were examined for pertinence to quantum dots (QDs).

The charge deep level transient spectroscopy (Q-DLTS) and transport measurements were used to characterize partially fluorinated films [31]. It has been found that at the temperature range from 330 to 250 K, the current is described by equation $I = I_o \exp(-E/kT)$, where E = 0.48 eV is the activation energy of the current flow through the film, and k is the Boltzmann constant. At lower temperatures, the current is close to be constant. The activationless current flow through the film is, most likely, associated with carrier migration (tunneling) through the traps in the FG band gap or graphene inclusions. Temperature dependence of the current is given in **Figure 7**, curve 1. Q-DLTS measurements demonstrate that only one type of activated process with energy 0.50 eV and density of localized states of ~ $10^{11}$ was observed. This activated process most likely corresponds to carriers passing over 0.5 eV potential barriers between graphene islands and fluorinated part of the film. It means that QDs with quantized electronic properties are not seen in these films. It may be connected with varying sizes of graphene islands and existing edge-related defects which provide the possibility of activationless transport in the films. It is worth mentioning that

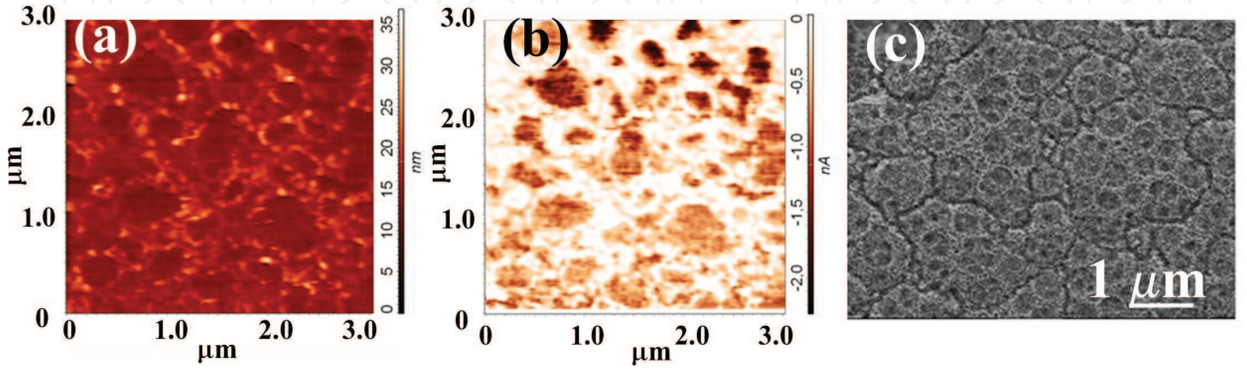


**Figure 5.** (a) AFM image of the FG film created by drops from a partially fluorinated suspension (7 days, $CF_{0.10}$) and (b) current map for the same place on the film. The bright regions in both images correspond to fluorinated graphene. (c) SEM image of the films created from a graphene suspension and treated in an aqueous solution of HF for 20 days ($CF_{0.23}$), respectively. Reprinted with permission from Ref. [31].

the arrays of QDs formed after similar fluorination of graphene or few layer graphene demonstrate the size quantization levels in Q-DLTS and transport measurements [31, 39–41]

## 6. Resistance switching effects in fluorinated films

Currently, the resistive memory approach is considered the most promising, as it allows obtaining a significantly lower time of memory operation (data overwriting). The most important parameters for the memory devices are a low overwriting voltage (lower than 3 V) and a high number of rewriting cycles and stability [42, 43]. The main problems of traditional metal oxide materials in the case of flexible electronics are relatively high fabrication temperature and very high cost. So, recent interest in the graphene-based materials results from its possible use for flexible resistive memory elements. Recently, some efforts have been made to create the resistive memory from graphene oxide (GO) or $MoS_2$/graphene oxide composite [5, 10]. We have investigated fluorographene that is much more stable than GO graphene derivatives. The resistive switching effect for partially fluorinated graphene films (a two-phase system of graphene islands embedded in FG matrix) was observed for the first time [32].

The reversible resistive switching effect was found for the films, created from the suspension of partially fluorinated graphene for fluorination level of about ~ $C_4F$ (fluorination time of 40–60 days). **Figure 6(a)** and **(b)** shows current-voltage (I-V) characteristics for vertical Au/FG/Si/InGa structures and lateral Au/FG/Au structures, measured at two voltage sweeps. It is seen that the transition to the lower resistance of the layer occurs at voltage of about −1.5 V in vertical configuration and at about −4 V in lateral configuration. The reverse transition occurs by changing the polarity of the applied voltage. Repeated measurements prove the repeatability of such switching. The variation of temperature measurements from 80 to 350 K shows that these transitions may be observed in the entire studied temperature range. Daylight illumination is very important for carrier transport in fluorinated films (compare **Figure 6(b)** and **(c)**). The reset loops observed in dark conditions degrade under daylight illumination. The reason for this effect is connected with a strong decrease in the time of nonequilibrium carrier relaxation, directly observed in similar structures [34].

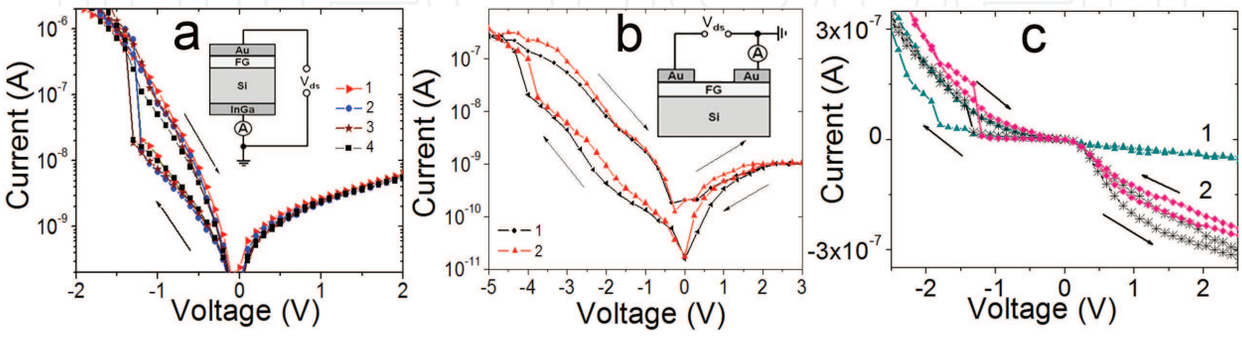


**Figure 6.** Current-voltage characteristics measured at daylight conditions of (a) vertical Au/FG/Si/InGa structures and (b) lateral Au/FG/Au structures (contact size was 0.5 mm, and period between contacts was 1.5 mm) measured several times at two voltage sweeps at the temperature of 300 K. (c) vertical Au/FG/Si/InGa structures measured in daylight (1) and dark (2) conditions. Fluorinated graphene film had thickness of 80 nm. Reprinted with permission from Ref. [32].

For a lower fluorination degree, the relation of resistances decreased, and for a higher fluorination degree, films became insulated.

One of the most important parameters of the material for resistive memory is the time of switching from high to low resistance states [5, 42, 43]. Q-DLTS measurements allow direct determination of the time of carrier emission (relaxation of nonequilibrium charge) from the specified traps [32]. Time is one of the switching process parameters. The emission (relaxation) time of nonequilibrium carriers is determined from the position of the corresponding peak on Q-DLTS spectrum. It was found that after applying relatively high voltage (~4 V) we can fix the low resistive state of films for Q-DLTS measurements, and after 160°C annealing, the high resistive state can be restored.

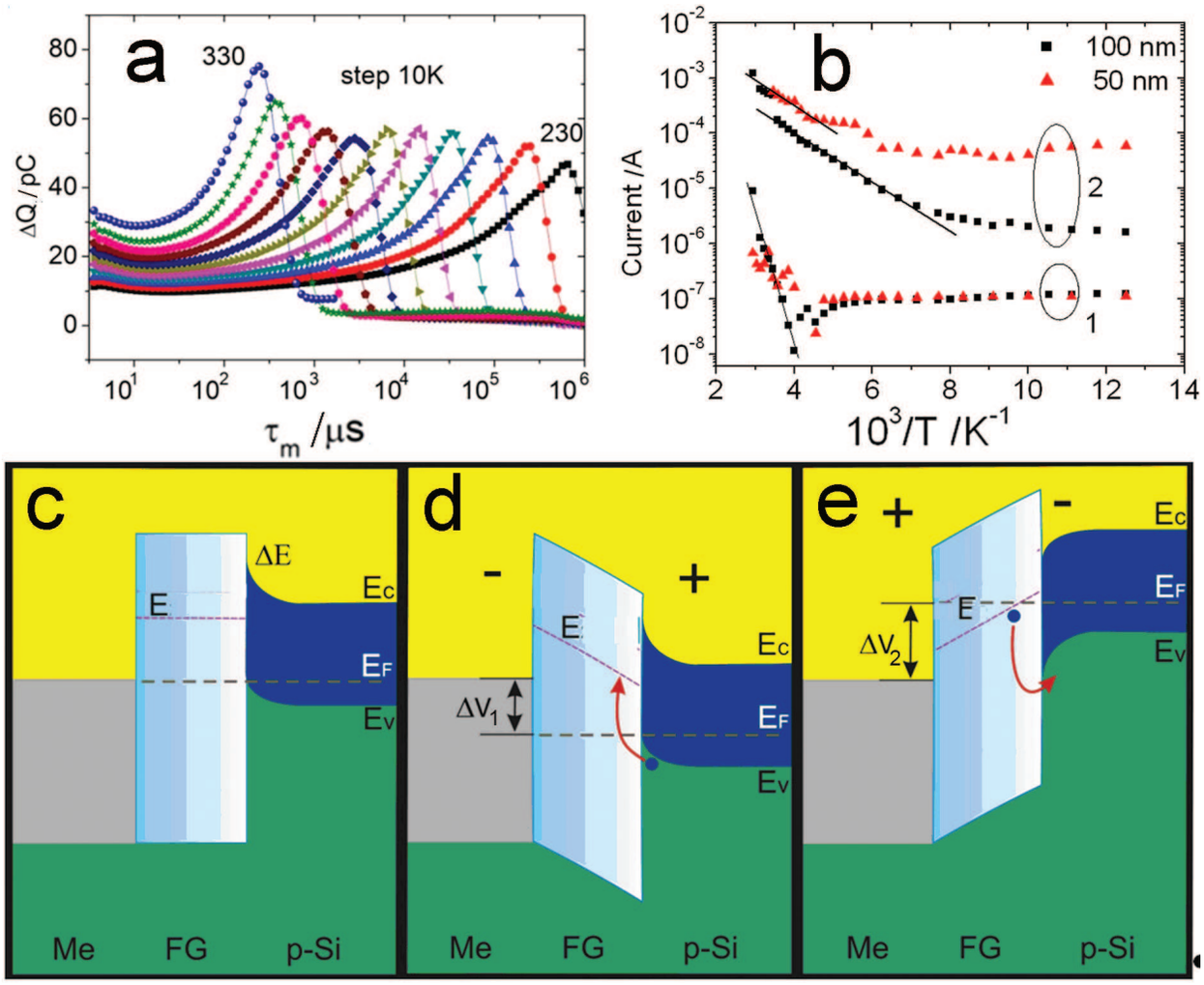


**Figure 7.** (a) Q-DLTS spectra for FG/p-Si structure in low resistance state, associated with the holes, which are consistent with the activation energy of the holes 0.34 eV in FG/p-Si structures. (b) Temperature dependences of the current through the fluorinated graphene film on p-Si substrate in the high (curve 1) and low (curve 2) resistance states, measured in vertical configuration. Lines correspond to the activation energy 0.48 eV (1) and 0.09 eV (2). (c–e) Expected band diagram of (c) Au/FG/p-Si structures at no voltage, (d) for the filling pulse $\Delta V_1$, (e) during the carriers emission from the traps for holes at constant voltage, applied to the sample $\Delta V_2$. Only one trap is considered in this diagram for simplicity. Reprinted with permission from Ref. [32].

The charge spectroscopy Q-DLTS and transport measurements were used to study traps in the films from partially fluorinated suspension in the states of both low and high resistance. The activation energy of traps $E_{01}$ (0.50 eV), obtained from Q-DLTS method for the films in high resistive states, as mentioned above, may be interpreted as a potential barrier between graphene and fluorinated graphene areas, or between FG film and valence bands of silicon substrate. Transport and nonequilibrium recharging processes in the high resistance state were found to occur above all, due to carrier tunnelling through potential barriers in the films. Several types of traps for electrons and holes (one trap is demonstrated in **Figure 7**) with the density of $10^{10}$–$10^{12}$ $cm^{-2}$ were formed in the low resistive state of FG films. Among them are electron traps with activation energies of 0.15, 0.12, and 0.08 eV, and hole traps with energy of 0.34 eV. The minimum relaxation time of nonequilibrium carriers from different traps was found to be about 700 ns. The energy level position of corresponding traps from the conduction band of a silicon substrate equals 0.08 eV. The origin of the observed traps is supposed to correspond to traces of organic components, which are used during graphene suspension creation.

**Figure 7(b)** demonstrates temperature dependences of the current through the films, with thickness of 50 nm and 100 nm, at two electric field intensities. For the low resistance state (curve 2), the activation energy E for both films with different thickness is 0.09 eV, at the temperature range from 330 to 150–170 K [32]. At lower temperatures, the current again is close to constant. The activationless current flow through the film is, most likely, associated with carrier tunneling on the traps in the FG band gap and graphene inclusions. Comparison of transport and Q-DLTS data demonstrates that the carrier transport in the low-resistance state is determined by the same traps (traps with activation energy 0.08 – 0.09 eV), and they form conductive channels in the films.

## 7. Films with negative differential resistance

Negative differential resistance (NDR) devices with nonohmic current-voltage characteristics are used in a wide range of applications, including frequency multipliers, memories, fast switches, high-frequency oscillators operating up to the THz range, etc., [44–46]. Currently, the theoretical predictions of NDR pertaining to graphene appear to prevail [47–49], and only a few experimental observations of NDR are presented in the literature (in fact, NDR is experimentally observed in lateral structures only in Ref. [50]). In the case of a two-barrier structure, it is possible to observe different regimes, from oscillation behavior in conductivity to only positive differential conductance [47]. It is this situation that was observed in our experiments for FG films with a relatively low fluorination degree (F/C ratio) [30].

In our case for films created from suspensions, NDR was observed for relatively weakly fluorinated layers $CF_x$ with fluorination degree ranged from $0.10 < x < 0.23$ (**Figure 8(a)** and **(b)**) [30]. Two types of the film with slightly different flake size demonstrate similar I-V curves, but with different numbers of peaks. These films demonstrate one or few peaks in I-V curves, depending on the flake sizes, and that is explained by formation of barrier or multi-barrier systems. The current steps also seen in I-V curves are most likely connected with the presence of electrically active traps considered above. It's worth noting that the obtained films were

multibarrier systems due to the presence of a fluorinated network and non-fluorinated graphene islands. An increase in the fluorination degree first results in the increased number of the FG barriers. The origin of NDR for I-V curves shown in **Figure 8(a)** and **(b)** is mostly likely associated with the theoretically predicted gap in the transmission coefficient for carriers in the barrier between fluorinated graphene and graphene areas. It is caused by the competition of hole-to-electron transport and Klein tunnelling with resonant tunnelling in structures with potential barrier(s) [48].

The origin of the NDR was demonstrated to vary with an increase in the F/C ratio. Thick FG films (150 nm) with F/G ratio $CF_{0.23}$ showed two peaks in the I-V curves, observed for voltages swept from negative to positive values (**Figure 8(c)** and **(d)**). The peaks were observed for the vertical configuration of measurements. A reverse voltage sweep produced I-V curves without any peaks (inset of **Figure 8(d)**). It is suggested that electrochemical oxidation-reduction reactions involving organic contaminants (traces of DMF, used to produce the graphene suspension) are located near defects, fluorinated carbons, or other special areas in our films. The temperature dependence of the conductivity at peaks exhibited activation behavior $\sigma = \sigma_0 \exp(-E_i/kT)$, where $E_i$ is the activation energy, k is the Boltzmann constant, and T is the temperature. $E_i$ takes values 0.04 and 0.09 for peak 1, and 0.16 for peak 2.

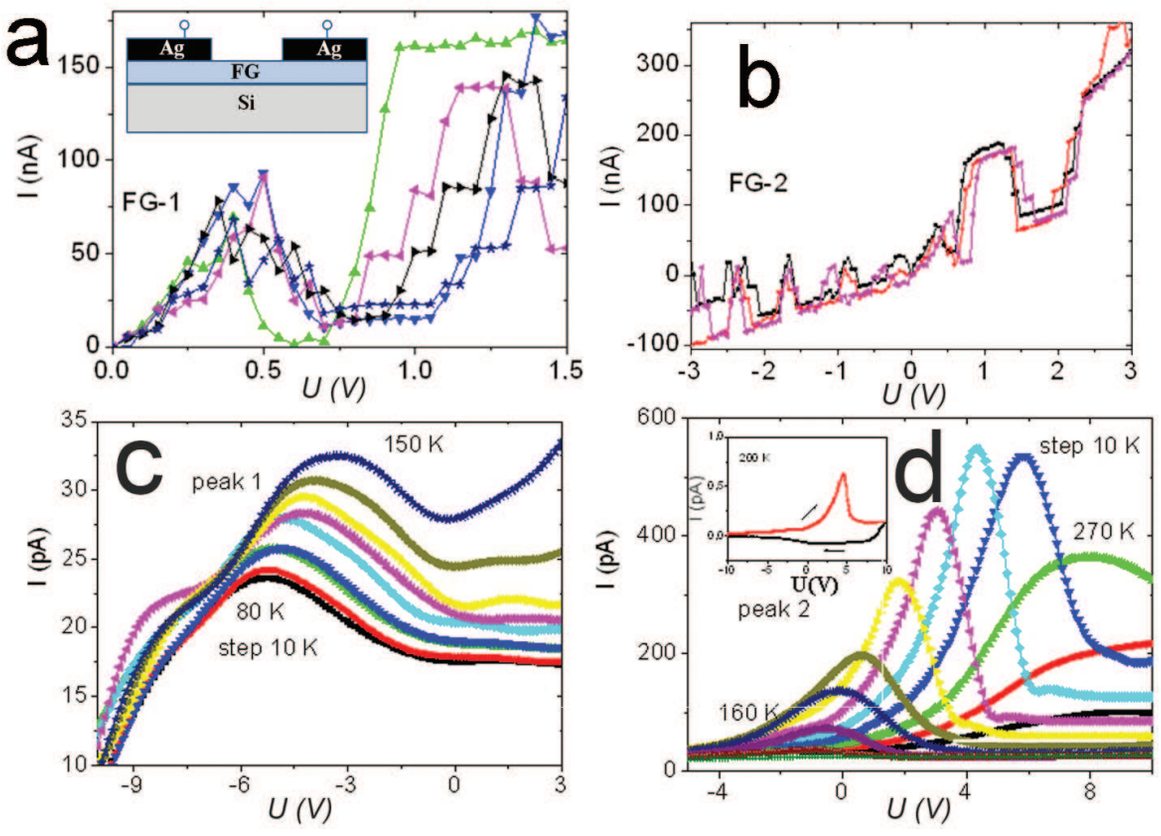


**Figure 8.** (a) and (b) I-V characteristics measured in lateral configurations for FG films ~$CF_{0.10}$ for films created from suspension with smaller flake size in the case (b). Different curves correspond to repeated measurements on the same structures. (c, d) I-V characteristics measured in vertical configuration for FG film ($CF_{0.23}$) over the temperature range of 80–300 K. Peak 1 (c) and peak 2 (d) were observed in thick 150 nm FG film. Reprinted with permission from Ref. [30].

http://dx.doi.org/10.5772/67451

The effect of NDR in fluorinated films widens the range of application including active device layers fabricated using 2D printed technologies on rigid and flexible substrates.

## 8. FG suspension for 2D inkjet printing technologies

The discovered control of the size of flakes in the graphene suspension during its fluorination serves to create inks for 2D inkjet printing [28, 51–53]. Suspensions of fluorinated graphene with nanometer size flakes are of interest for the development of 2D inkjet printing technologies, and production of thermally and chemically stable dielectric films for nanoelectronics [28]. The printed fluorinated graphene films on silicon and flexible substrates have been demonstrated first time, and the charges in MIS structures have been estimated as ultra low values of (0.5–2) × $10^{10}$ $cm^{-2}$.

The properties of the graphene oxide films may be greatly improved by adding the FG top layer. The thin FG and GO films are printed on silicon and flexible polyethylene terephthalate (PET) substrates (**Figure 9 (a)** and **(b)**). FG flakes have lateral sizes ranging within 20–100 nm and thickness of 0.4–1.5.nm. **Figure 9 (a)** contains the photo of printed graphene oxide lines with different number of layers. Layers in the left part of the substrate are coated by a layer of printed FG. The boundary between areas with and without FG is marked with arrows. The FG

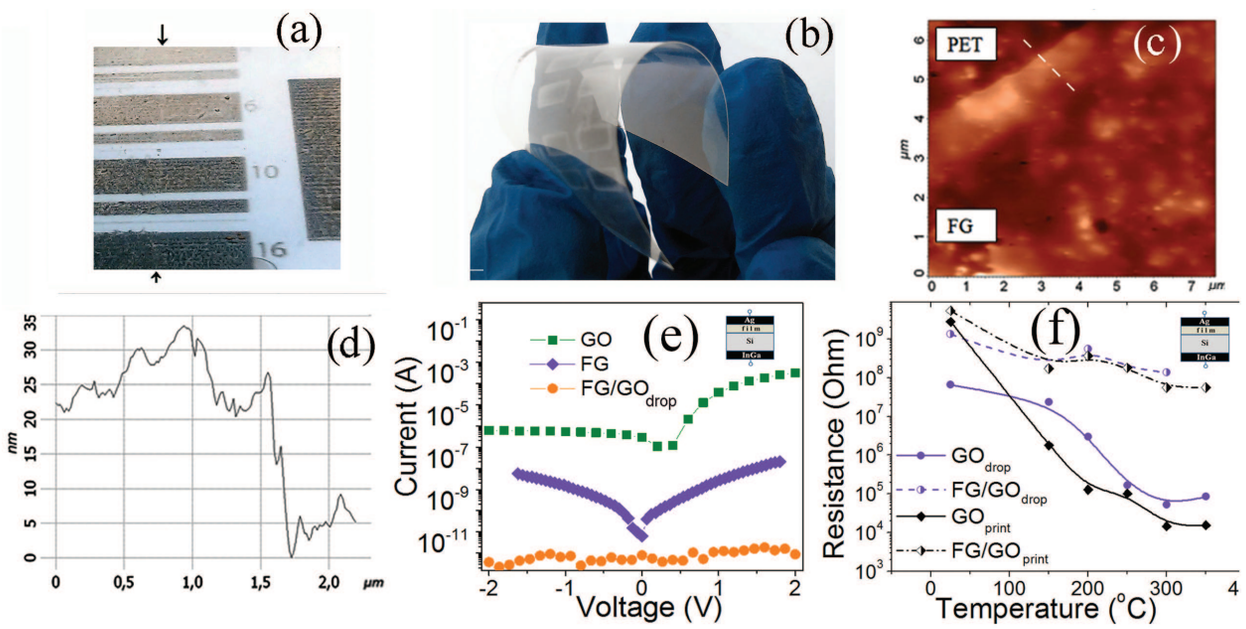


**Figure 9.** (a) FG printed 10-layer films on the PET substrate. (b) Images of graphene oxide printed 4, 6, 10, and 16-layer films with an additional FG 8-layered coating printed on top of the left half of the wafer. The boundary of the FG layer is slightly seen in the image, and for better visualization, it is marked with arrows. (c) An AFM image and height profile (d) near the edge of the FG film from (b). FG layer thickness can be estimated at ~17 nm. (e) Comparison of the current values through the GO, FG, and FG/GO films deposited by droplets. (f) Dependence of the current through the two-layer FG/GO and GO films on the isochronous (20 min) annealing temperature; the considered films were obtained by printing and applying droplets. Annealings were carried out in an inert atmosphere (Ar with addition of 10% $H_2$). Reprinted with permission from Ref. [28].

layers on the PET substrate are presented in **Figure 9 (b)**. An AFM image of the FG layer on PET and the profile near the edge of FG film are demonstrated in **Figure 9 (c)** and **(d)**.

The properties of two-layer films of FG on GO were the most extensively studied due to their revealed stability. **Figure 9 (e)** shows the current-voltage characteristics of the two-layer films of FG/GO, created by printing and dropping, measured in lateral configuration. It has been found out that the magnitude of the current through the two-layer structure is significantly lower than that through the separate films of GO or FG. The increase in the two-layer film thickness was shown to be not that significant, compared with the effect of reducing the current through the film by several orders of magnitude, especially in the case of printed layers. Applying the FG layer causes primarily the "healing" of structural defects in the GO film. The origin of this effect lies in good affinity between GO and FG, and in the electrostatic interaction between GO structural defects and FG flakes. Surface roughness of different films on rigid substrates was extracted from AFM images: the surface roughness for GO film was 8.1 nm, for FG/GO film, it was 5.7 nm, and for FG film, it was 1.5 nm. This effect is supposed to result from blocking of graphene oxide conductivity with small FG flakes. Significant decrease in FG/GO film roughness suggests formation of FG few layers on structural defects of GO films (local insulating island with thickness exceeding the average FG film thickness).

Assessment of thermal stability of different structures required investigation and comparison of the conductivity of GO and FG/GO films, obtained by applying drops and printing. **Figure 9** (f) presents dependences of film resistance on temperature of isochronous annealing. The graphs show that the resistance of the two-layer structures, both printed and created by drops, changes not more than by 1–1.5 orders, while the change in the resistance of the graphene oxide films in both cases is 3–5 orders of magnitude. Therefore, the two-layer FG/GO films are much more stable than the GO films, since the application of the second layer greatly suppresses the GO recovery during heating.

## 9. Outlook and conclusion remarks

Creation of the fluorinated graphene suspension and inks are shown to extend the range of graphene-based materials from conductive to insulating and functional layers (**Figure 10**). The suggested approach for graphene or graphene suspension fluorination in the aqueous solution of hydrofluoric acid allows obtaining the partially fluorinated graphene with fluorine content lower than in $CF_{0.5}$. This approach is cheap, practically feasible, and easy to produce. Moreover, films obtained from the partially fluorinated graphene may be conducting or insulating, depending on the suspension fluorination degree.

Fluorinated graphene cannot be structured using traditional technological approaches such as plasma treatment. This problem of the fluorinated graphene nanostructuring is successfully overcome by means of spin-coating or printed technologies. As a result, the use of FG suspension is the most convenient approach for a wide spectrum of applications, especially for flexible technologies.

http://dx.doi.org/10.5772/67451

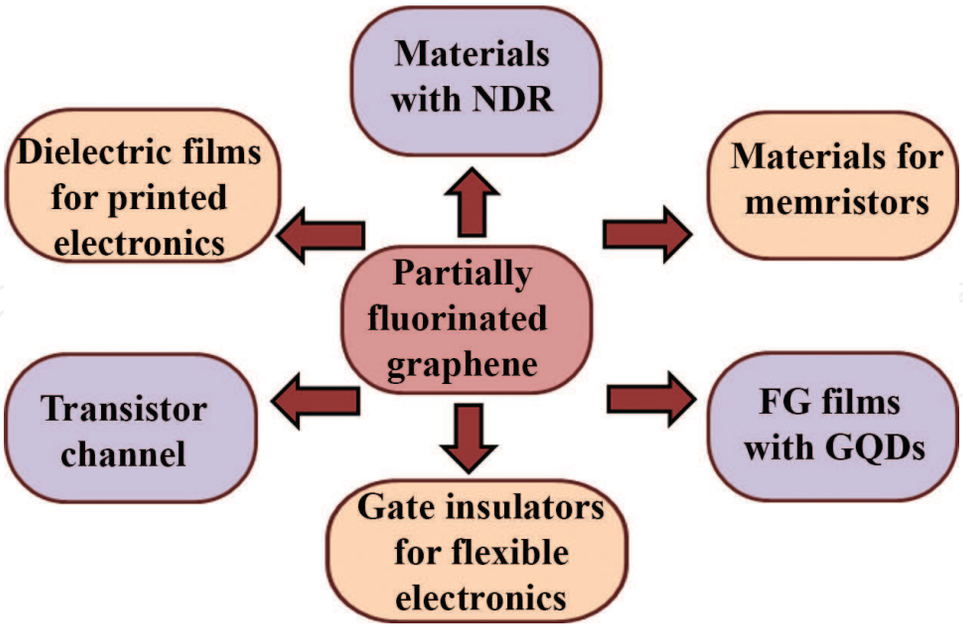


**Figure 10.** Schematic illustration of possible applications for partially fluorinated graphene films created from suspensions.

The fluorination process in the case of graphene suspension causes additional flakes splitting and fragmentation. The small size of the fluorinated flakes makes them an excellent base for graphene-based inks. Dropped and printed films, obtained from the inks both on rigid and flexible substrates, demonstrate a great potential for a wide spectrum of electronic devices, especially for flexible electronics. Partial fluorination provides for FG films such effects as NDR and resistive switching that are promising for applications. The development of optimized dielectrics for the graphene active layer (active layer gate and interlayer dielectrics or/and substrate for graphene) has been described. Dielectric layers fabricated from fluorinated graphene or in combination with graphene oxide are the most promising graphene-based flexible and transparent electronics.

## Acknowledgements

The study was financially supported by the Russian Science Foundation, grant 15-12-00008. **Figures 1**, **3**, and **4** are reproduced from Ref. [20] with permission from the PCCP Owner Societies.

## Author details

Irina V. Antonova* and Nadezhda A. Nebogatikova

*Address all correspondence to: nadonebo@gmail.com, antonova@isp.nsc.ru

A. V. Rzhanov Institute of Semiconductor Physics, SB RAS, Novosibirsk State Technical University, Novosibirsk, Russia

## References

[1] Han X, Chen Y, Zhu H, Preston C, Wan J, Fang Z, Hu L: Scalable, printable, surfactant-free graphene ink directly from graphite. Nanotechnology. 2013;**24**:205304. DOI: 10.1088/0957-4484/24/20/205304

[2] Wei D, Li H, Han D, Zhang Q, Niu L, Yang H, Bower C, Andrew P, Ryhänen T: Properties of graphene inks stabilized by different functional groups. Nanotechnology. 2011;**22**:245702. DOI: 10.1088/0957-4484/22/24/245702

[3] Lee CL, Chen CH, Chen CW: Graphene nanosheets as ink particles for inkjet printing on flexible board. Chem. Eng. J. 2013;**230**:296–2. DOI: 10.1016/j.cej.2013.06.093

[4] Secor EB, Prabhumirashi PL, Puntambekar K, Geier ML, Hersam MC: Inkjet printing of high conductivity flexible graphene patterns. J. Phys. Chem. Lett. 2013;**4**:1347–51. DOI: 10.1021/jz400644c

[5] Antonova IV: Non-organic dielectric layers for graphene and flexible electronics. Int. J. Nanomater. Nanotechnol. Nanomed. 2016;**2**:018–24. DOI: 10.17352/2455-3492.000010

[6] Song L, Ci L, Lu H, Sorokin PB, Jin C, Ni J, Kvashnin AG, Kvashnin DG, Lou J, Yakobson BI, Ajayan PM: Large scale growth and characterization of atomic hexagonal boron nitride layers. Nano Lett. 2010;**10**:3209–15. DOI: 10.1021/nl1022139

[7] Eda G, Fanchini G, Chhowalla M: Large-area ultrathin films of reduced graphene oxide as a transparent and flexible electronic material. Nat. Nanotechnol. 2008;**3** 270−4. DOI: 10.1038/nnano.2008.83

[8] Standley B, Mendez A, Schmidgall E, Bockrath M: Graphene−graphite oxide field-effect transistors. Nano Lett. 2012;**12**:1165−9. DOI: 10.1021/nl2028415

[9] Petrone N, Chari T, Meric I, Wang L, Shepard KL, Hone J: Flexible graphene field-effect transistors encapsulated in hexagonal boron nitride. ACS Nano. 2015;**9**:8953–9. DOI: 10.1021/acsnano.5b02816

[10] Lee GH, Yu YJ, Cui X, Petrone N, Lee CH, Choi MS, Lee DY, Lee C, Yoo WJ, Watanabe K, Taniguchi T, Nuckolls C, Kim P, Hone J: Flexible and transparent $MoS_2$ field-effect transistors on hexagonal boron nitride graphene heterostructures. ACS Nano. 2013;**7**:7931–6. DOI: 10.1021/nn402954e

[11] Lee SK, Kim BJ, Jang H, Yoon SC, Lee C, Hong BH, Rogers JA, Cho JH, Ahn JH: Stretchable graphene transistors with printed dielectrics and gate electrodes. Nano Lett. 2011;**11**:4642–6. DOI: 10.1021/nl202134z

[12] Lee SK, Jang HY, Jang S, Choi E, Hong BH: All graphene-based thin film transistors on flexible plastic substrates. Nano Lett. 2012;**12**:3472−6. DOI: 10.1021/nl300948c

[13] Jewel MU, Siddiquee TA, Islam MR. Flexible graphene field effect transistor with graphene oxide dielectric on polyimide substrate. In: Proceeding of the International

Conference on Electrical Information and Communication Technology (EICT); 13–15 February 2013; Khulna, Bangladesh: IEEE; 2013. pp. 1–5. DOI: 10.1109/EICT.2014.6777834

[14] Nair RR, Ren W, Jalil R, Riaz I, Kravets VG, Britnell L, Blake P, Schedin F, Mayorov AS, Yuan S, Katsnelson MI, Cheng HM, Strupinski W, Bulusheva LG, Okotrub AV, Grigorieva IV, Grigorenko AN, Novoselov KS, Geim AK: Fluorographene: a two dimensional counterpart of Teflon. Small. 2010;**6**:2877–84. DOI: 10.1002/smll.201001555

[15] Robinson JT, Burgess JS, Junkermeier CE, Badescu SC, Reinecke TL, Perkins FK, Zalalutdniov MK, Baldwin JW, Culbertson JC, Sheehan PE, Snow ES: Properties of fluorinated graphene films. Nano Lett. 2010;**10**:3001–5. DOI: 10.1021/nl101437p

[16] Ho KI, Huang CH, Liao JH, Zhang W, Li LJ, Lai CS, Su CY: Fluorinated graphene as high performance dielectric materials and the applications for graphene nanoelectronics. Sci. Rep. 2014;**4**:5893. DOI: 10.1038/srep05893

[17] Lee W-K, Robinson JT, Gunlycke D, Stine RR, Tamanaha CR, King WP, Sheehan PE: Chemically isolated graphene nanoribbons reversibly formed in fluorographene using polymer nanowire masks. Nano Lett. 2011;**11:**5461–4. DOI: 10.1021/nl203225w

[18] Nebogatikova NA, Antonova IV, Komonov AI, Prinz VY: Producing arrays of graphene and few-layer graphene quantum dots in a fluorographene matrix. Optoelectronics, Instrumentation and Data Processing. 2014:**50**:298–303. DOI: 10.3103/S8756699014030145

[19] Nebogatikova NA, Antonova IV, Volodin VA, Prinz VY: Functionalization of graphene and few-layer graphene with aqueous solution of hydrofluoric acid. Phys. E. 2013;**52**:106–11. DOI: 10.1016/j.physe.2013.03.028

[20] Nebogatikova NA, Antonova IV, Prinz VY, Kurkina II, Alexandrov GN, Timofeev VB, Smagulova SA, Zakirov ER, Kesler VG: Fluorinated graphene dielectric films obtained from functionalized graphene suspension: preparation and properties. Phys. Chem. Chem. Phys. 2015;**17**:13257–66. DOI: 10.1039/C4CP04646C

[21] O'Neill A, Khan U, Nirmalraj PN, Boland J, Coleman JN: Graphene dispersion and exfoliation in low boiling point solvents. J. Phys. Chem. C. 2011;**115**:5422-8. DOI: 10.1021/jp110942e

[22] Wang J, Manga KK, Bao Q, Loh KP: High-yield synthesis of few-layer graphene flakes through electrochemical expansion of graphite in propylene carbonate electrolyte. J. Am. Chem. Soc. 2011;**133**:8888–91. DOI: 10.1021/ja203725d

[23] Su CY, Lu AY, Xu Y, Chen FR, Khlobystov AN, Li LJ: High-quality thin graphene films from fast electrochemical exfoliation. ACS Nano. 2011;**5**:2332–9. DOI: 10.1021/nn200025p

[24] Zhou M, Tang J, Cheng Q, Xu G, Cui P, Qin LC: Few-layer graphene obtained by electrochemical exfoliation of graphite cathode. Chem. Phys. Lett. 2013;**572**:61–5. DOI: 10.1016/j.cplett.2013.04.013

[25] Lotya M, Hernandez Y, King PJ, Smith RJ, Nicolosi V, Karlsson LS, Blighe FM, De S, Wang Z, McGovern IT, Duesberg GS, Coleman JN: Liquid phase production of graphene by

exfoliation of graphite in surfactant/water solutions. J. Am. Chem. Soc. 2009;**131**:3611–20. DOI: 10.1021/ja807449u

[26] Shinde DB, Brenker J, Easton CD, Tabor RF, Neild A, Majumder M: Shear assisted electrochemical exfoliation of graphite to graphene. Langmuir. 2016;**32**:3552–9. DOI: 10.1021/acs.langmuir.5b04209

[27] Paton KR, Varrla E, Backes C, Smith RJ, Khan U, Neill AO, Boland C, Lotya M, Istrate OM, King P, Higgins T, Barwich S, May P, Puczkarski P, Ahmed I, Moebius M, Pettersson H, Long E, Coelho J, O'Brien SE, McGuire EK, Sanchez BM, Duesberg GS, McEvoy N, Pennycook TJ, Downing C, Crossley A, Nicolosi V, Coleman JN: Scalable production of large quantities of defect-free few-layer graphene by shear exfoliation in liquids. Nat. Mater. 2014;**13**:624–30. DOI: 10.1038/nmat3944

[28] Nebogatikova NA, Antonova IV, Kurkina II, Soots RA, Vdovin VI, Timofeev VB, Smagulova SA, Prinz VY: Fluorinated graphene suspension for inkjet printed technologies. Nanotechnology. 2016;**27**:205601. DOI: 10.1088/0957-4484/27/20/205601

[29] dos Santos RB, Rivelino R, Mota FB, Gueorguiev GK: Exploring hydrogenation and fluorination in curved 2D carbon systems: a density functional theory study on Corannulene. J. Phys. Chem. A. 2012;**116**:9080−7. DOI: 10.1021/jp3049636

[30] Nebogatikova NA, Antonova IV, Prinz VY, Timofeev VB, Smagulova SA: Graphene quantum dots in fluorographene matrix formed by means of chemical functionalization. Carbon. 2014;**77**: 1095–103. DOI: 10.1016/j.carbon.2014.06.026

[31] Antonova IV, Kurkina II, Nebogatikova NA, Smagulova SA. Films fabricated from partially fluorinated graphene suspension: structural, electronic properties and negative differential resistance. Nanotechnology. 2017;**28**:074001. DOI: 10.1088/1361-6528/28/7/074001

[32] Kurkina II, Antonova IV, Nebogatikova NA, Kapitonov AN, Smagulova SA: Resistive switching effect and traps in partially fluorinated graphene films. Journal of Physics D: Applied Physics. 2016;**49**:095303. DOI: 10.1063/1.4953239

[33] Liu HY, Hou ZF, Hu CH, Yang Y, Zhu ZZ. Electronic and magnetic properties of fluorinated graphene with different coverage of fluorine. J. Phys. Chem. C. 2012;**116**:18193−201. DOI: 10.1021/jp303279r

[34] Duan Y, Stinespring CD, Chorpening B: Electronic structures, bonding configurations, and band-gap-opening properties of graphene binding with low-concentration fluorine. Chem. Open. 2015;**4**:642–50. DOI: 10.1002/open.201500074

[35] Hoex B, Gielis JJH, Van de Sanden MCM, Kessels WMM: On the *c*-Si surface passivation mechanism by the negative-charge-dielectric $Al_2O_3$. J. Appl. Phys. 2008;**104**:113703. DOI: 10.1063/1.3021091

[36] Garg R, Chowdhury NA, Bhaskaran M, Swain PK, Misra D. Electrical characteristics of thermally evaporated $HfO_2$. J. Electrochem. Soc. 2004;**151**:F215–9. DOI: 10.1149/1.1784212

[37] Terlinden NM, Dingemans G, Vandalon V, Bosch RHEC, Kessels WMM. Influence of the $SiO_2$ interlayer thickness on the density and polarity of charges in $Si/SiO_2/Al_2O_3$ stacks as studied by optical second-harmonic generation. J. Appl. Phys. 2014;**115**:033708. DOI: 10.1063/1.4857075

[38] Hasan M, Jang M, Kim D-H, Nguyen MC, Yang H, Jeong JK, Choi R. Improved electrical properties of solution-processed $ZrO_2$ gate dielectric for large-area flexible electronics. Jap. J. Appl. Phys. 2013;**52**:100206. DOI: 10.7567/JJAP.52.100206

[39] Antonova IV, Nebogatikova NA, Prinz VY: Self-organized arrays of graphene and few-layer graphene quantum dots in fluorographene matrix: charge transient spectroscopy. Appl. Phys. Lett. 2014;**104:**193108. DOI: 10.1063/1.4878262

[40] Antonova IV, Nebogatikova NA, Prinz VY, Popov VI, Smagulova SA: Light-assisted recharging of graphene quantum dots in fluorographene matrix. J. Appl. Phys. 2014;**116:**134310. DOI: 10.1063/1.4897231

[41] Antonova IV, Nebogatikova NA, Prinz VY: Fluorinated graphene films with graphene quantum dots for electronic applications. J. Appl. Phys. 2016;**119;**224302. DOI: 10.1063/1.4953239

[42] Yang JJ, Zhang MX, Strachan JP, Miao F, Pickett MD, Kelley RD, Medeiros-Ribeiro G, Williams RS: High switching endurance in TaOx memristive devices. Appl. Phys. Lett. 2010;**97**:232102. DOI: 10.1063/1.3524521

[43] Jeong DS, Thomas R, Katiyar RS, Scott JF, Kohlstedt H, Petraru A, Hwang CS: Emerging memories: resistive switching mechanisms and current status. Reports on Progress in Physics. 2012;**75**:076502. DOI: 10.1088/0034-4885/75/7/076502

[44] Lyo IW, Avouris P: Negative differential resistance on the atomic scale: implications for atomic scale devices. Science. 1989;**245**:1369–71. DOI: 10.1126/science.245.4924.1369

[45] Chen J, Reed MA, Rawlett AM, Tour JM: Large on-off ratios and negative differential resistance in a molecular electronic device. Science. 1999;**286**:1550–2. DOI: 10.1126/science.286.5444.1550

[46] Léonard F, Tersoff J: Negative differential resistance in nanotube devices. J. Phys. Rev. Lett. 2000;**85**:4767–70. DOI: 10.1103/PhysRevLett.85.4767

[47] Song Y, Wu HC, Guo Y: Negative differential resistance in graphene double barrier resonant tunneling diode. Appl. Phys. Lett. 2013;**102**:093118. DOI: 10.1063/1.4794952

[48] Nguyen HC,Nguyen VL: Tunneling of dirac electrons through one-dimensional potentials in graphene: a T-matrix approach. J. Phys.: Condens. Matter. 2009;**21**:045305. DOI: 10.1088/0953-8984/21/4/045305

[49] Ren H, Li QX, Luo Y, Yang JL: Graphene nanoribbon as a negative differential resistance device. Appl. Phys. Lett. 2009;**94**:173110. DOI: 10.1063/1.3126451

[50] Wu Y, Farmer DB, Zhu W, Han SJ, Dimitrakopoulos CD, Bol AA, Avouris P, Lin YM. Three-terminal graphene negative differential resistance devices. ACS Nano. 2012;**6**:2610–2. DOI: 10.1021/nn205106z

[51] Kamyshny A, Magdassi S: Conductive nanomaterials for printed electronics. Small. 2014;**10**:3515–35. DOI: 10.1002/smll.201303000

[52] Li J, Ye F, Vaziri S, Muhammed M, Lemme MC, Östling M: Efficient inkjet printing of graphene. Adv. Mater. 2013;**25**:3985-92. DOI: 10.1002/adma.201300361

[53] Xu Y, Hennig I, Freyberg D, Strudwick AJ, Schwab MG, Weitz T, Cha KCP: Inkjet-printed energy storage device using graphene/polyaniline inks. J. Power Sources. 2014;**248**:483–8. DOI: 10.1016/j.jpowsour.2013.09.096